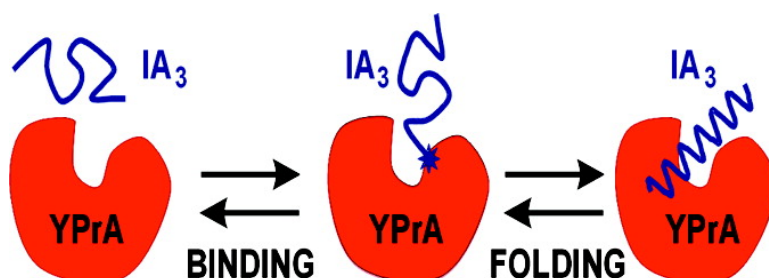Article

Kinetics of Folding and Binding of an Intrinsically Disordered Protein: The Inhibitor of Yeast Aspartic Proteinase YPrA

Ranjani Narayanan, Omjoy K. Ganesh, Arthur S. Edison, and Stephen J. Hagen

More About This Article

Additional resources and features associated with this article are available within the HTML version:

- Supporting Information
- Access to high resolution figures
- Links to articles and content related to this article
- Copyright permission to reproduce figures and/or text from this article

View the Full Text HTML

Kinetics of Folding and Binding of an Intrinsically Disordered Protein: The Inhibitor of Yeast Aspartic Proteinase YPrA

Ranjani Narayanan,[†] Omjoy K. Ganesh,[‡] Arthur S. Edison,[‡] and Stephen J. Hagen*,[†]

Physics Department and Department of Biochemistry and Molecular Biology, University of Florida, P.O. Box 118440, Gainesville FL 32611-8440

Received April 30, 2008; E-mail: sjhagen@ufl.edu

Abstract: The 68 residue peptide IA$_3$ is an intrinsically unstructured protein that serves as an endogenous inhibitor of the yeast aspartic proteinase A (YPrA). Although unstructured in free solution, IA$_3$ forms an N-terminal α helix as it binds to YPrA, leading to subnanomolar inhibition of the protease. Equilibrium structural and inhibition studies provide little insight into the mechanism and kinetics of the coupled folding and binding interaction. We have used laser temperature jump spectroscopy to study the kinetics of folding of free IA$_3$ and of the interaction between IA$_3$ and YPrA. Inducing folding with trifluoroethanol cosolvent allows us to determine the folding rate ($k_f \approx 0.3\ (\mu s)^{-1}$) and the unfolding rate ($k_u \approx 3\ (\mu s)^{-1}$) for free IA$_3$ in water at 25 °C. A substantially faster relaxation process is observed in the presence of the proteinase; this process appears to be the kinetic signature of an intermediate binding step in the coupled folding and binding interaction of IA$_3$ and YPrA.

Introduction

Recent estimates suggest that as many as 30% of eukaryotic proteins contain large, unstructured regions under physiological conditions.[1−9] These regions undergo a disordered-to-ordered transition upon binding to target biomolecules. Such intrinsically disordered proteins (IDPs) play a key role in various cellular functions, including the regulation of transcription and translation and the modulation of the activity and assembly of proteins.[2,5,6,10] It has been argued that the absence of a stable structure may confer a number of benefits to protein function; these benefits may include enhanced flexibility to interact with multiple targets, greater tolerance to environmental changes (pH, temperature), and the possibility of regulation *via* proteolysis.[1,6,10,11] It has also been suggested that the disorder of an IDP may accelerate its binding to a target molecule by expanding the capture radius for nonspecific or non-native interactions (the

Scheme 1
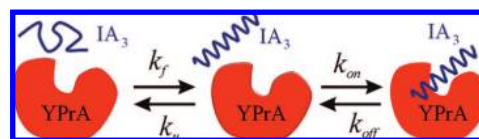
Scheme 2
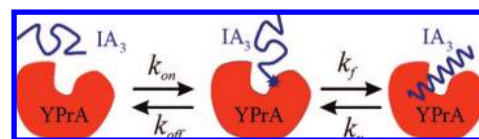
"fly casting" model).[12] The fact that the amino acid sequence of an IDP does not lead to a unique and stable fold *in vivo*, and that the lack of stable structure may actually enhance the functionality of some proteins, poses an intriguing challenge to the classic structure−function paradigm for proteins.[1,2,11]

Although there is a growing literature on the identification and characterization of IDPs and their complexes, the kinetics and mechanisms of their coupled folding and binding interactions are little understood. The sequence of events in binding, the presence (or absence) of intermediate states and the kinetics of the relevant transitions are generally not known. Perhaps the simplest question one can ask is whether the IDP folds prior to binding the target (Scheme 1), or whether it first associates as a disordered peptide and then folds, with the target acting as a template for folding (Scheme 2). More complex descriptions are of course possible,[13] but testing even crude models is already difficult because most folding and binding interactions have very

† Physics Department.
‡ Department of Biochemistry and Molecular Biology.
(1) Wright, P. E.; Dyson, H. J. *J. Mol. Biol.* **1999**, *293* (2), 321–331.
(2) Uversky, V. N.; Gillespie, J. R.; Fink, A. L. *Proteins: Struct., Funct., Genet.* **2000**, *41* (3), 415–427.
(3) Dunker, A. K.; Cortese, M. S.; Romero, P.; Iakoucheva, L. M.; Uversky, V. N. *FEBS J.* **2005**, *272* (20), 5129–5148.
(4) Dyson, H. J.; Wright, P. E. *Nat. Rev. Mol. Cell Biol.* **2005**, *6* (3), 197–208.
(5) Fink, A. L. *Curr. Opin. Struct. Biol.* **2005**, *15* (1), 35–41.
(6) Uversky, V. N.; Oldfield, C. J.; Dunker, A. K. *J. Mol. Recognit.* **2005**, *18* (5), 343–384.
(7) Le Gall, T.; Romero, P. R.; Cortese, M. S.; Uversky, V. N.; Dunker, A. K. *J. Biomol. Struct. Dyn.* **2007**, *24* (4), 325–341.
(8) Radivojac, P.; Iakoucheva, L. M.; Oldfield, C. J.; Obradovic, Z.; Uversky, V. N.; Dunker, A. K. *Biophys. J.* **2007**, *92* (5), 1439–1456.
(9) Xie, H. B.; Vucetic, S.; Iakoucheva, L. M.; Oldfield, C. J.; Dunker, A. K.; Uversky, V. N.; Obradovic, Z. *J. Proteome Res.* **2007**, *6* (5), 1882–1898.
(10) Dyson, H. J.; Wright, P. E. *Curr. Opin. Struct. Biol.* **2002**, *12* (1), 54–60.
(11) Dunker, A. K.; et al. *J. Mol. Graphics Modell.* **2001**, *19* (1), 26–59.

(12) Shoemaker, B. A.; Portman, J. J.; Wolynes, P. G. *Proc. Natl. Acad. Sci. U.S.A.* **2000**, *97* (16), 8868–8873.

fast kinetics. Very few experimental studies have shed light on mechanisms of coupled folding and binding.[14−17] Sugase et al. investigated the folding of the intrinsically unstructured pKID domain of the transcription factor CREB as it interacts with the KIX domain of the CREB binding protein.[14] They found evidence for multiple nonspecific, primarily hydrophobic contacts between pKID and its target, occurring in a series of fast kinetic stages that precede the much slower formation of the folded or native contacts. This result supports a model in which an encounter complex is rapidly stabilized by a variety of nonnative interactions, prior to development of the native interactions. Very recently, Onitsuka et al. studied two very slow-folding IDP mutants of staphylococcal nuclease (SNase) that fold upon binding to their target ligand.[15] They found that one mutant folds prior to binding the ligand, while the other binds the ligand and then folds. Evidently the folding/binding mechanisms for different IDPs may be qualitatively different. It is quite unknown which mechanism may be more common.

The 68-residue peptide IA$_3$ from *Saccharomyces cerevisiae* is the endogenous inhibitor of yeast aspartic proteinase A (YPrA, saccharopepsin), and YPrA appears to be the sole inhibitory target of IA$_3$.[18,19] IA$_3$ is found in the cytosol of *S. cerevisiae*, whereas the proteinase YPrA is sequestered in the acidic vacuoles (pH ≈ 4.5).[20,21] Since IA$_3$ binds to YPrA with subnanomolar affinity, it is postulated that cytosolic IA$_3$ protects the cell by inhibiting YPrA in the event of a vacuole rupture.[20] Equilibrium circular dichroism (CD) and NMR studies have shown that free IA$_3$ is intrinsically disordered.[22,23] However, X-ray crystallography of the IA$_3$-YPrA complex shows that residues 2−32 of IA$_3$ fold into an α-helix that binds just above the active site cleft of YPrA (PDB ID: 1DPJ, 1DP5), blocking access to the active site (Figure 1).[24] Therefore, the interaction of IA$_3$ with its target constitutes a unique mode of enzyme inhibition in which the proteinase folds its own inhibitor into a helix.[24] The same study also showed that a truncated IA$_3$ consisting only of the N-terminal residues 2−34 forms the same helix on YPrA, inhibiting the protease with equal affinity.[24,25] That is, the C-terminal residues 35−68 appear unnecessary for inhibitory function. Interestingly, although IA$_3$ efficiently inhibits YPrA, it does not inhibit other proteases that are structurally or
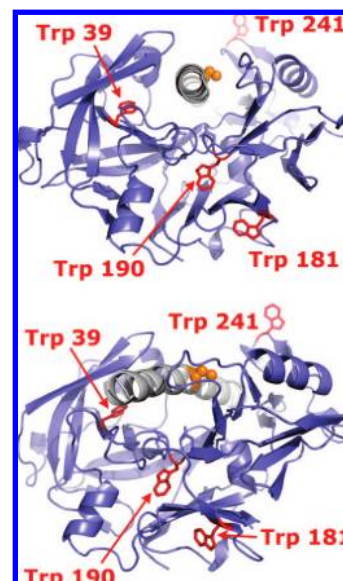

Figure 1. Two views of an X-ray model of the inhibition complex of YPrA (blue) and IA$_3$ (gray), based on the 1DPJ and 1DP5 crystal structures (24). The N-terminal residues of IA$_3$ form a helix over the enzyme catalytic site; the view along the IA$_3$ helix is toward the N-terminus (with K32 of IA$_3$ near the front and M1 at the rear). The four native tryptophans of YPrA are shown in red, and the cysteine residue introduced in the K16C mutant of IA$_3$ is modeled in orange. The figure shows only the helical N-terminus of IA$_3$, as only residues 3−31 (1DPJ) or 2−32 (1DP5) of IA$_3$ are seen in the crystal structures.

sequentially similar to YPrA; in fact it is typically cleaved by such enzymes.[24,25]

We have used laser temperature-jump fluorescence spectroscopy (*T*-jump) and fluorescence resonance energy transfer (FRET) to investigate the folding and binding interaction of IA$_3$ and YPrA. Our method consists of three steps. The first step is to use circular dichroism spectroscopy to measure the unfolding free energy of the IA$_3$ helix in the presence of the helix-inducing cosolvent TFE (2,2,2,-trifluoroethanol). We then use laser temperature-jump (*T*-jump) spectroscopy to measure the rate of folding of free IA$_3$ as a function of TFE concentration. Extrapolating the measured folding and unfolding rates to aqueous solvent conditions reveals the folding rate of free IA$_3$ in water. The third step is to measure the relaxation kinetics of the IA$_3$/YPrA complex in response to a laser *T*-jump in water. Significantly faster relaxation kinetics were observed in the complex than in the free peptide, consistent with a model in which IA$_3$ forms a disordered encounter complex with the proteinase, prior to folding (Scheme 2). This result, together with existing prior work on similar systems,[14,15] suggests that template-driven folding may be a common mechanism by which IDPs interact with their targets.

Materials and Methods

Peptide Design for Fluorescent Probes. To study the kinetics of free IA$_3$ folding we constructed a double mutant of the full length peptide, N2W−K16C, labeled with a FRET donor and acceptor. The tryptophan at position 2 acts as a FRET donor, and the cysteine residue at position 16 provides an attachment site for a dansyl moiety acting as FRET acceptor (Figure 2). The tryptophan absorbs at 250−290 nm and emits with a fluorescence peak near 350 nm. The dansyl primarily absorbs near 336 nm and emits its fluorescence near 495 nm. For the donor−acceptor pair, the literature value of

(13) Wang, J.; Zhang, K.; Lu, H. Y.; Wang, E. K. *Phys. Rev. Lett.* **2006**, *96*, (16).
(14) Sugase, K.; Dyson, H. J.; Wright, P. E. *Nature* **2007**, *447* (7147), 1021–1025.
(15) Onitsuka, M.; Kamikubo, H.; Yamazaki, Y.; Kataoka, M. *Proteins: Struct., Funct., Bioinf.* **2008**, *72* (3), 837–847.
(16) Muralidhara, B. K.; Rathinakumar, R.; Wittung-Stafshede, P. *Arch. Biochem. Biophys.* **2006**, *451* (1), 51–58.
(17) Meisner, W. K.; Sosnick, T. R. *Proc. Natl. Acad. Sci. U.S.A.* **2004**, *101* (37), 13478–13482.
(18) Dreyer, T.; Valler, M. J.; Kay, J.; Charlton, P.; Dunn, B. M. *Biochem. J.* **1985**, *231* (3), 777–779.
(19) Parr, C. L.; Keates, R. A. B.; Bryksa, B. C.; Ogawa, M.; Yada, R. Y. *Yeast* **2007**, *24* (6), 467–480.
(20) Lenney, J. F.; Wiemken, A.; SCHELLEN, M.; Meyer, J. *Biochem. Biophys. Res. Commun.* **1974**, *60* (4), 1378–1383.
(21) Hasilik, A.; Muller, H.; Holzer, H. *Eur. J. Biochem.* **1974**, *48* (1), 111–117.
(22) Ganesh, O. K.; Green, T. B.; Edison, A. S.; Hagen, S. J. *Biochemistry* **2006**, *45* (45), 13585–13596.
(23) Green, T. B.; Ganesh, O.; Perry, K.; Smith, L.; Phylip, L. H.; Logan, T. M.; Hagen, S. J.; Dunn, B. M.; Edison, A. S. *Biochemistry* **2004**, *43* (14), 4071–4081.
(24) Li, M.; Phylip, L. H.; Lees, W. E.; Winther, J. R.; Dunn, B. M.; Wlodaawer, A.; Kay, J.; Gustchina, A. *Nat. Struct. Biol.* **2000**, *7* (2), 113–117.
(25) Phylip, L. H.; Lees, W. E.; Brownsey, B. G.; Bur, D.; Dunn, B. M.; Winther, J. R.; Gustchina, A.; Li, M.; Copeland, T.; Wlodawer, A.; Kay, J. *J. Biol. Chem.* **2001**, *276* (3), 2023–2030.

Figure 2. Mutant IA₃ peptides used in this study. A dansyl label introduced at C16 is a FRET acceptor for a tryptophan donor introduced at position 2. The sequence of the K16C-dansyl single mutant (not shown) is identical (except for the absence of W2) to that of the double mutant shown here.

Table 1. Native Tryptophan Residues in YPrA and Their Distances from the FRET-Acceptor Label of Bound IA₃[a]

YPrA residue	IA₃ K16C-dansyl distance (nm)
W39	1.9
W181	2.8
W190	1.8
W241	1.8

[a] Values are $C_\alpha - C_\alpha$ distances, derived from the 1DPJ and 1DP5 crystal structures of the YPrA/IA₃ complex.[24]

the Förster radius is 2.2 nm,[26] which is similar to the $C_\alpha - C_\alpha$ separation of 2.03 nm between residues N2 and K16 in the folded N-terminus of IA₃. This separation is expected to increase upon melting of the helix, leading to reduced FRET efficiency, so that (under UV excitation) unfolding of IA₃ should yield an enhanced Trp emission signal.

Bimolecular FRET served as a probe of the IA₃-YPrA interaction. The FRET acceptor was a labeled single mutant (K16C-dansyl) of IA₃, while the four native tryptophan residues of the wildtype YPrA (Figure 1) acted as FRET donors. In the crystal structure of IA₃ bound to YPrA, three of the YPrA tryptophan residues (W39, W190, and W241) lie within the 2.2 nm Förster radius of a dansyl moiety attached to residue 16 of the IA₃ helix (Figure 1 and Table 1). Residue W181 of YPrA lies at a distance of 2.8 nm away.

Peptide Purification, Labeling, and Characterization. IA₃ was expressed in *Escherichia* as described by Phylip et al.[25] with a C-terminal histidine tag to aid in purification by metal affinity chromatography. As an unstructured protein, IA₃ can withstand boiling or freezing conditions that typically denature and aggregate structured proteins. Cell lysates from protein expression were boiled and then rapidly cooled to room temperature and then centrifuged at 27 000 g. A 0.2 μm filter separated the supernatant from aggregated protein, and the filtrate was loaded onto a nickel column (SIGMA Nickel-NTA) pre-equilibrated with 50 mM phosphate buffer (pH 8.0). The column was then washed with two column volumes of phosphate buffer at pH 8.0, followed by two column volumes of phosphate buffer at pH 6.3 containing 10% glycerol. Purified histidine tag IA₃ was eluted from the column with phosphate buffer at pH 4. Molecular weight was verified by MALDI mass spectrometry and SDS-PAGE analysis. The purified protein was then dialyzed to water and lyophilized.

The dansyl label, in the form of 1,5-IAEDANS (Invitrogen I-14), was attached to the cysteine residue of the IA₃ K16C single mutant and N2W−K16C double mutant. The IA₃ mutant was equilibrated with TCEP (tris (2-carboxyethyl) phosphine) to hinder disulphide bond formation between cysteine residues. 1,5-IAEDANS dissolved in dimethylformamide was added to the protein solution and stirred under a nitrogen atmosphere for 2 h at room temperature. Pure labeled protein was separated from the reaction mixture by reverse phase chromatography on a Vydac C-18 column. Dansyl-labeling

of the IA₃ K16C single mutant and N2W−K16C double mutant was verified by MALDI mass spectrometry.

Lyophilized YPrA was purchased from Sigma (P-8892) and rehydrated in 0.1 M sodium acetate buffer at pH 4.5. SDS-PAGE and gel filtration chromatography confirmed the purity of the protease.

Inhibition Assay. Inhibition assays verified that our mutations and dansyl-labeling did not significantly alter the inhibitory action of IA₃ against YPrA. Inhibitory activity of the single- and double-labeled IA₃ mutants was tested by a kinetic assay that uses the chromogenic substrate RS6.[27,28] Inhibition constants for all mutants were at or beyond limits of instrument detection at 25 °C and pH 4.5, implying $K_I < 1$ nM as seen in the wild type IA₃.[25]

Circular Dichroism (CD) Measurements. Equilibrium far-UV circular dichroism (CD) spectra were collected for wild type IA₃ and for all of the mutants in this study (N2W, K16C, N2W−K16C), at ~15 μM concentration in pH 7.0 phosphate buffer and in varying concentrations of TFE. Spectra were collected on an Aviv-202 circular dichroism spectrometer at wavelengths 190−245 nm, with TFE concentrations of 0−25% v/v and temperatures of 5−85 °C in 5 °C increments. A reference (buffer) spectrum was subtracted from each CD spectrum.

Fitting the CD Spectra. To find the TFE-dependence of the folding stability of the free IA₃ helix, we fit the CD spectra to a two-state thermodynamic model in which the free energy of helix unfolding ΔG shifts linearly with the addition of TFE:[29]

$$\Delta G = \Delta H - T\Delta S$$
$$\Delta H = \Delta H_0 + m_H[\text{TFE}]$$
$$\Delta S = \Delta S_0 + m_S[\text{TFE}] \tag{1}$$

The unfolding free energy of a given mutant is then characterized by two enthalpy parameters, ΔH_0 and m_H, and two entropy parameters, ΔS_0 and m_S. In order to fit CD spectra to such a model, two base lines (representing ellipticity at 100% helix and at 100% coil) are customarily defined; CD data can then be converted to values of percent helix.[30] However, our large set of ellipticity data, covering multiple wavelengths, temperatures, and TFE concentrations for each peptide, allowed us instead to use a global fit to determine the enthalpy and entropy of unfolding and the wavelength-dependent baseline spectra.

The global fit makes no assumptions about either the helix or coil CD spectra, except that the helix (and coil) spectrum of each peptide is both temperature- and TFE-independent and that the helix and coil convert through a two-state transition: If $\Theta(\lambda,T,\text{TFE})$ is the ellipticity at wavelength λ, temperature T, and at a given TFE concentration, then the global fit assumes that

$$\Theta(\lambda,T,\text{TFE}) = \Theta_f(\lambda) \times f_f(T,\text{TFE}) + \Theta_u(\lambda) \times f_u(T,\text{TFE}) \tag{2}$$

Here $\Theta_f(\lambda)$ is the ellipticity of the fully folded state, $\Theta_u(\lambda)$ is the ellipticity of the fully unfolded state, and $f_f = 1 - f_u$ is the fraction of molecules folded:

$$f_f = 1/(1 + \exp(-\Delta G/RT)) \tag{3}$$

If the solvent condition is indicated by the parameter X - i.e. one value of X describes one experimental condition of T and [TFE], then $\Theta(\lambda,X)$ is a matrix of measured ellipticities, $\Theta_f(\lambda)$ and $\Theta_u(\lambda)$ can be expressed as column vectors, and $f_f(X)$ and $f_u(X)$ can be expressed as row vectors. Equation 2 can be written as a matrix equation

$$\Theta(\lambda, X) = [\Theta_f(\lambda)\Theta_u(\lambda)]\begin{bmatrix} f_f(X) \\ f_u(X) \end{bmatrix} \tag{4}$$

(26) Wu, P. G.; Brand, L. *Anal. Biochem.* **1994**, *218* (1), 1–13.

(27) Dunn, B. M.; Kammermann, B.; Mccurry, K. R. *Anal. Biochem.* **1984**, *138* (1), 68–73.

(28) Kondo, H.; Shibano, Y.; Amachi, T.; Cronin, N.; Oda, K.; Dunn, B. M. *J. Biochem.* **1998**, *123* (1), 141–147.

(29) Jasanoff, A.; Fersht, A. R. *Biochemistry* **1994**, *33* (8), 2129–2135.

(30) Luo, P. Z.; Baldwin, R. L. *Biochemistry* **1997**, *36* (27), 8413–8421.
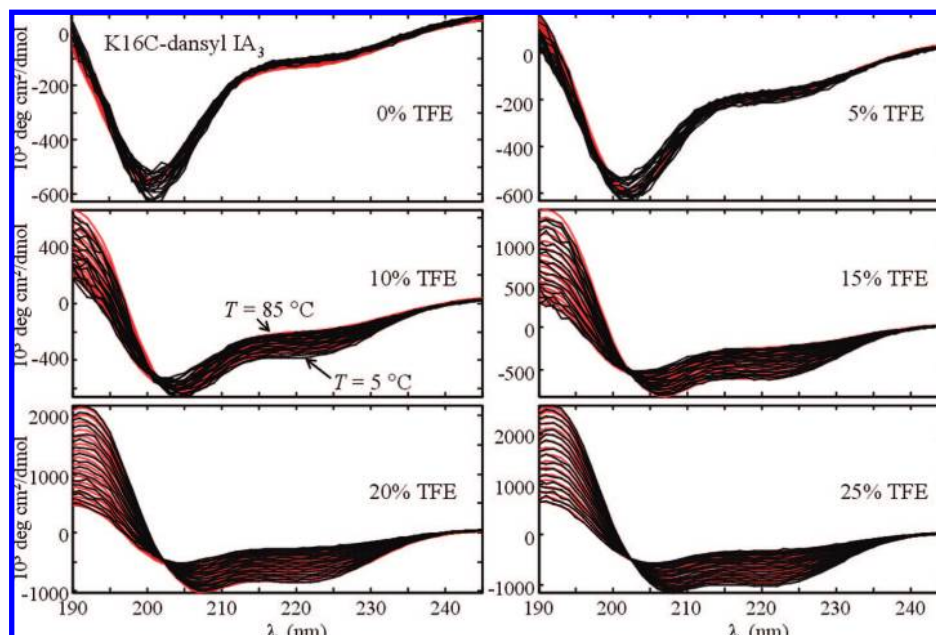
Figure 3. Far-UV circular dichroism spectra (black curves) for single-labeled K16C-dansyl IA$_3$, as a function of wavelength, TFE concentration, and temperature. Temperature ranged from 5 to 85 °C in steps of 5 °C. Red curves show the global fit to the equilibrium model (eq 1 and 2), which gives the thermodynamic parameters in Table 2. CD data and fit results for the other three peptides were very similar.

Given the experimental data $\Theta(\lambda, X)$ and the fraction folded f_f (X) for a particular peptide, one can directly solve eq 4 (in a least-squares sense) to find $\Theta_f(\lambda)$ and $\Theta_u(\lambda)$. Therefore the global fit proceeds as follows: (1) Choose starting values for the equilibrium thermodynamic parameters (ΔH_0, ΔS_0, m_H, and m_S); (2) Given those values, calculate the fraction folded f_f for all experimental conditions (T and [TFE]); (3) Use the data $\Theta(\lambda, T, \text{TFE})$ and the calculated f_f (T, TFE) to solve eq 4 to give the basis spectra Θ_u and Θ_f; (4) Generate from eq 2 the predicted CD spectra as a function of λ, T, and [TFE]; (5) calculate the residual between the CD prediction and data; (6) adjust the thermodynamic parameters and return to step 2.

This routine produced a very satisfactory fit to the CD data for the WT IA$_3$ and all mutants. We did however find that an additional 15−20% reduction in the sum of squares was possible if the unfolded state spectrum $\Theta_u(\lambda)$ was allowed to vary linearly with [TFE]: $\Theta_u(\lambda, \text{TFE}) = \Theta_u(\lambda) + \alpha(\lambda)$ [TFE].

This introduces a term with $\alpha(\lambda)$ into eq 2 but does not otherwise affect the fitting procedure significantly. It has minor effect on free energy parameters (e.g., ΔG changes by $\sim$0.2 RT). Figure 3 shows representative spectra and the fit. Figure 4 shows that the resulting unfolded-state basis spectra depend only weakly on the TFE concentration (i.e., that $\alpha(\lambda)$ is small at all wavelengths). Table 2 gives the results of the fits.

Equilibrium Fluorescence. Equilibrium fluorescence spectra were recorded on a JASCO FP-750 spectrofluorometer at 25 °C for free tryptophan (NATA, N-acetyl-tryptophan-amide) and for the Trp and dansyl-labeled mutants of IA$_3$, at 15 μM concentration and with excitation at 270 nm, in phosphate buffer with TFE concentrations from 0 to 25% v/v TFE (Figure 5). Samples were sealed to prevent evaporation of TFE.

Temperature-Jump Spectroscopy. The laser T-jump instrument[31] uses a pump−probe method to time-resolve the changes in the sample fluorescence emission following rapid thermal excitation by an IR laser pulse. The 1064 nm fundamental of an Nd:YAG laser pulse is Raman-shifted to 1890 nm in a H$_2$ cell, and the shifted pulse is then split into two counter-propagating pulses that enter the aqueous sample. The IR laser pulse generates a temperature
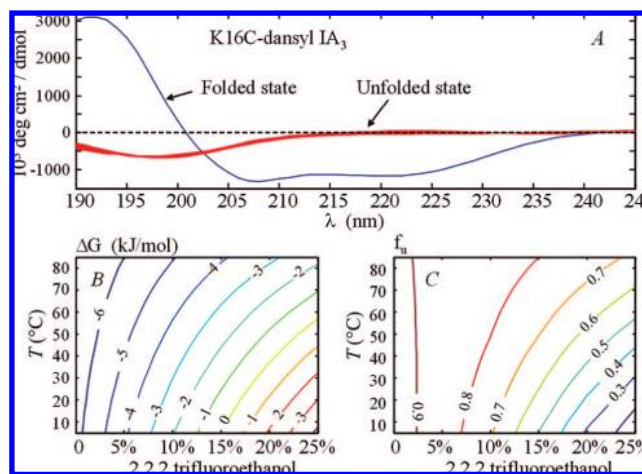
(31) Qiu, L. L.; Pabit, S. A.; Roitberg, A. E.; Hagen, S. J. *J. Am. Chem. Soc.* **2002**, *124* (44), 12952−12953.

Figure 4. Results of global fit to CD spectra, for single-labeled peptide, K16-dansyl IA$_3$. Results for the other three peptides were very similar. (A) Folded and unfolded state spectra $\Theta_f(\lambda)$ and $\Theta_u(\lambda)$ (see eq 2 and 4) derived from global fit. The fitting model allows a TFE-dependence in the unfolded state spectrum $\Theta_u(\lambda)$, so that the red curve is actually the family of curves representing $\Theta_u(\lambda, \text{TFE})$ over the range 0−25% TFE. (B) Contour map showing free energy of unfolding, as calculated from the fit parameters in Table 2. (C) Equilibrium fraction of molecules unfolded, $f_u(T, \text{TFE})$ as calculated from fit parameters.

jump of 5−10 °C within 20−30 ns in the sample, which flows continuously through a silica capillary (100 μm path length). At a time delay t following the IR pulse, a laser pulse at 266 nm excites the fluorescence of the sample. The emitted light is collected by two detectors. The first detector is a photomultiplier (Hamamatsu R1166), which records the overall Trp emission intensity through a short pass filter. The second detector is a CCD array (Roper MicroMax), which records the dispersed spectrum generated as the emission strikes a diffraction grating. This allows us to collect time-resolved emission spectra that span the wavelength range 290−725 nm, for time delays t from $\sim$30 ns to $\sim$1 ms following the T-jump. At longer time scales the thermal recovery of the sample begins. The fluorescence of a reference sample of free tryptophan (NATA) is used to calibrate the magnitude of the temperature jump.

Table 2. Folding Free Energy Parameters for Labeled Mutants of Free IA₃, from Two-State Fit to CD Spectra[a]

Peptide	ΔH_0 kJ/mol	ΔS_0 kJ/mol/K	m_H kJ/mol/ [TFE]	m_S kJ/mol/K/[TFE]	ΔG (aq, 25 °C) (kJ/mol)	[TFE]$_{mid}$
WT	−6.39	0.00164	135	0.332	−6.9	0.193
N2W	−5.34	0.00475	126	0.309	−6.8	0.197
K16C-dansyl	−3.99	0.00821	123	0.291	−6.4	0.178
N2W−K16C-dansyl	−2.44	0.0119	99.5	0.229	−6.0	0.192

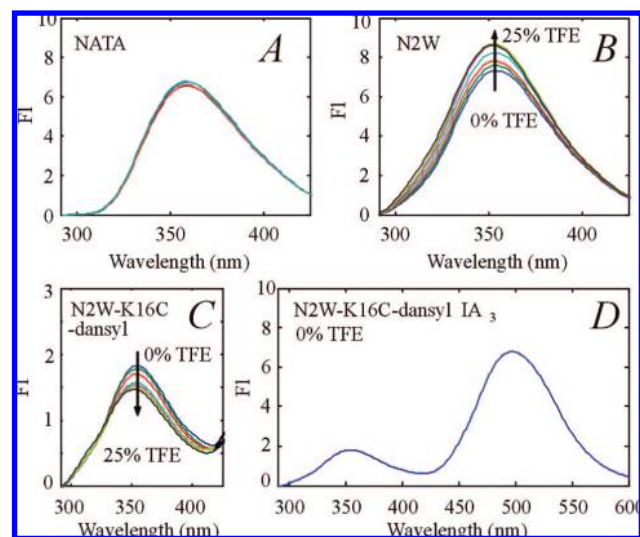[a] [TFE] is expressed as a volume fraction, i.e. [TFE] = 0.1 for 10% v/v.

Figure 5. Equilibrium fluorescence spectra under excitation at 270 nm in varying concentrations of TFE. (Concentrations in panels A−C are 0, 5, 8, 12, 17, 20, and 25% TFE v/v.) (A) Emission of 15 μM *N*-acetyl tryptophan amide (NATA) at *T* = 25 °C is independent of TFE concentration over the range 0−25% TFE (v/v). (B) Under the same solvent conditions the Trp emission of the single-labeled mutant N2W IA₃ shows rising emission as TFE is added to induce the helical fold. (C) In the double-labeled (Trp donor and dansyl acceptor) mutant N2W−K16C-dansyl IA₃, the Trp emission declines as TFE is added, consistent with fluorescence resonance energy transfer from the Trp donor to the dansyl acceptor in the helical state. (D) The double labeled mutant N2W−K16C-dansyl IA₃ shows emission at both 350 nm (Trp) and 500 nm (dansyl). The figure shows the emission for 270 nm excitation in aqueous solvent at room temperature. The dansyl peak rises with the addition of TFE, consistent with a FRET signature of helix folding. However, the use of 270 nm excitation leads to some direct excitation of the dansyl, making it less reliable than Trp as an indicator of donor/acceptor separation.

***T*-Jump Data−Decomposition of Spectra.** Time-resolved fluorescence spectra from *T*-jump experiments were decomposed by singular value decomposition (SVD),[32,33] prior to fitting. If the matrix $A(\lambda,t)$ describes the measured emission intensities at a set of wavelengths λ and delay times t, then SVD decomposes A into a matrix of orthonormal wavelength basis vectors $U(\lambda)$ and a matrix of orthonormal time courses $V(t)$:

$$A(\lambda,t) = U(\lambda)SV(t)^T \qquad (5)$$

S is a diagonal matrix with elements arranged in descending order. S_n, which is the *n*th diagonal element of S, gives the weight for the *n*th basis spectrum $U_n(\lambda)$ and its time course $V_n(t)$ in the decomposition of $A(\lambda,t)$. U_n and V_n are the *n*th columns of the matrices U and V respectively.

The fluorescence spectra in our kinetic measurements of free IA₃ folding typically contained three significant SVD components. The fluorescence signal shows a very rapid drop from its pretrigger level during the 20−30 ns duration of the *T*-jump IR pulse, as fluorescence quantum yields typically fall as the temperature rises.

In the nanoseconds and microseconds that follow, the amplitude and wavelength of the fluorescence spectrum shift as the peptide population reequilibrates at the new temperature. We fit this relaxation to a single exponential process with relaxation time $\tau = 1/k_{relax}$, as follows:

$$S_nV_n(t) = a_n + b_n\exp(-t/\tau) \qquad (6)$$

Here a_n and b_n are constants. The fit requires the same value of τ for all SVD components. (Thermal recovery of the sample to its pretrigger temperature occurs on a slower ($\geq$ms) time scale).

Results

Equilibrium Stability of Free IA₃. The stabilization of helical secondary structure by 2,2,2-trifluoroethanol (TFE), even in peptides that have little or no helical content in the absence of TFE, has been well-studied.[29,30,34] For peptides that lack helical structure in water, the folding equilibrium can be characterized as a function of TFE concentration and a suitable extrapolation can establish the helix-coil equilibrium constants in water.[29,30] Equilibrium far-UV circular dichroism (CD) served as our probe of the helix-coil transition in four mutants of IA₃ as a function of TFE concentration and temperature. Figure 3 shows CD spectra collected for the K16C-dansyl mutant of IA₃. At low TFE concentrations the spectra show a dominant minimum near 200 nm, characteristic of a disordered peptide. As the TFE concentration rises to 20−25% the spectrum develops weak minima near 208 and 220 nm, characteristic of α-helical secondary structure. The presence of an isodichroic point near 202 nm in the CD spectra for all of the IA₃ mutants suggests a two-state character for the coil-helix transition, consistent with NMR chemical shift studies.[22,23] We therefore used a two-state model to fit the CD spectra for each peptide and obtain the free energy of helix unfolding as a function of solvent conditions, $\Delta G(T, [TFE])$ (see Materials and Methods).

Figures 3 and 4 show the results of the two-state fit to the CD spectra of the K16C-dansyl mutant (see Materials and Methods). For this mutant and for all others, agreement between the measured spectra and the two-state fit is quite good at all wavelengths, temperatures, and TFE concentrations studied. For each mutant the unfolding midpoint occurs near 18 or 19% TFE at 25 °C, consistent with the value [TFE]$_{mid} \approx 0.18$ obtained from NMR chemical shift measurements on wildtype IA₃[22] (Table 2). Figure 4, which is based on the CD fit results for K16C-dansyl IA₃, shows a contour map of the unfolding free energy and the fraction of molecules unfolded, versus *T* and [TFE]. Similar contour maps are found for the other mutants in this study. One striking feature of the contours at low TFE concentrations is that they lie nearly parallel to the *T*-axis, indicating that the enthalpy of folding is very small in the absence of TFE. Hence *T*-jump experiments conducted in plain buffer (0% TFE) are unlikely to provide a strong folding/unfolding signal in the free peptide. In order to measure the folding kinetics by *T*-jump, it is necessary to add TFE cosolvent,

(32) Henry, E. R.; Hofrichter, J. *Methods Enzymol.* **1992**, *210*, 129–192.
(33) Hendler, R. W.; Shrager, R. I. *J. Biochem. Biophys. Methods* **1994**, *28*, 1–33.

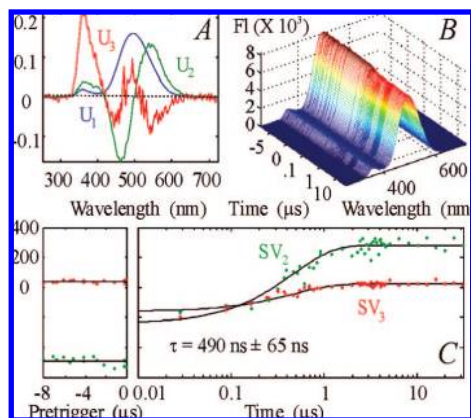(34) Buck, M. *Q. Rev. Biophys.* **1998**, *31* (3), 297–355.

Figure 6. Laser temperature-jump measurement of fluorescence spectra of double-labeled mutant N2W−K16C-dansyl IA₃ free in solution with 17% TFE. The laser *T*-jump occurs at time *t* = 0 and increases the temperature abruptly from 17.3 to 24.2 °C within 20−30 ns. (A) Spectral decomposition finds three significant components $U_1(\lambda)$ − $U_3(\lambda)$ in the time-resolved emission spectra shown in panel (B). (C) Time-dependence components of spectral decomposition, $SV_2(t)$ and $SV_3(t)$ (associated with the spectral components $U_2(\lambda)$ and $U_3(\lambda)$ respectively), show a single relaxation time τ = 490 ± 65 ns following the *T*-jump trigger.

to induce a greater enthalpy of unfolding, and then extrapolate the observed rates down to conditions of low TFE concentration.

_T_-Jump Study of Folding Kinetics of Free IA₃ Peptide. Figure 6 shows the relaxation of the fluorescence emission spectrum of the double-labeled peptide, N2W−K16C-dansyl, in a TFE/buffer mixture following a laser *T*-jump. The perturbation triggers a very rapid (<20−30 ns) decrease in overall fluorescent emission, followed by a slower (∼500 ns) relaxation. The rapid initial decrease - which is observed even in free tryptophan (NATA) - reflects the intrinsic temperature dependence of the fluorescence quantum yield and is not relevant to folding kinetics. The subsequent relaxation is best studied through an SVD analysis of the spectra (see Materials and Methods), where it appears in the second and third components SV_2 and SV_3; these describe the time-course of the spectral components $U_2(\lambda)$ and $U_3(\lambda)$ respectively. The rise of both SV_2 and SV_3 on the same time scale indicates that the 500 ns relaxation corresponds to rising emission by the Trp donor (350 nm) and a declining emission (and frequency shift) by the dansyl acceptor (500 nm). Hence the FRET efficiency declines, consistent with helix unfolding at the elevated temperature. As anticipated from the contour maps of Figure 4, little if any folding/unfolding signal is detected in the double-labeled peptide in the absence of TFE. Fitting the relaxation of SV_2 and SV_3 to an exponential time course (eq 6) gives the relaxation time constant $\tau = 1/k_{relax}$.

The interpretation of this time constant in terms of two-state kinetics requires some caution. Helix-coil transitions can exhibit deviations from two-state equilibrium behavior and from two-state kinetics.[35,36] Deviations may include nonexponential kinetics and a weak (or absent) temperature dependence of the relaxation rate; these deviations can be interpreted in terms of the separate relaxation and equilibration processes for nucleation vs. propagation of the helical conformation along the sequence.[37] This system, however, shows a strongly two-state character in
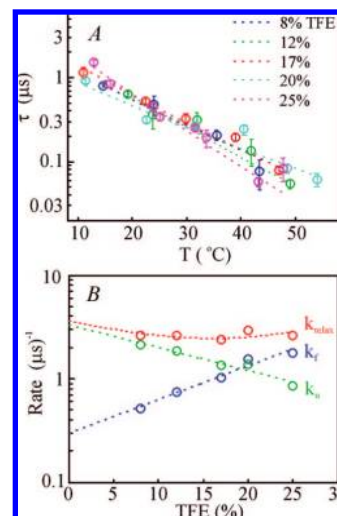

Figure 7. Kinetics results from *T*-jump study of double mutant N2W−K16C-dansyl IA₃: (A) Time constant (τ = $1/k_{relax}$) of exponential relaxation observed in Trp/dansyl fluorescence, following *T*-jump to temperature *T*. The observed rates show temperature dependence but little sensitivity to TFE concentration. Dashed lines indicate a simple Arrhenius fit for each TFE concentration; (B) For data at 25 °C, the rates of folding (k_f) and unfolding (k_u) are extracted from k_{relax} through a two-state model (eq 7). Extrapolation (dashed lines) to 0% TFE gives k_u = 3.3 ± 0.5 (μs)$^{-1}$, k_f = 0.30 ± 0.04 (μs)$^{-1}$ in water at 25 °C.

the equilibrium spectroscopy (CD and NMR) as well as a strongly temperature-dependent, and relatively slow (see below), relaxation rate τ (Figure 7). These findings suggest that the helix of IA₃ nucleates sufficiently slowly, relative to its propagation, that folding is satisfactorily approximated by a two-state model. In this case the relaxation time τ is related to the rates of helix folding (k_f) and unfolding (k_u) by

$$1/\tau = k_{relax} = k_f + k_u \qquad (7)$$

The ratio $k_f/k_u = \exp(\Delta G(T,TFE)/RT)$ was evaluated for each solvent condition from the thermodynamic parameters (Table 2), so that the measured τ and eq 7 could then be solved for k_f and k_u at each solvent condition. Figure 7 shows that these rates fall on a straight line on a semilogarithmic scale. (This is expected if the addition of TFE induces a linear shift in the free energy barriers for folding and unfolding. A linear shift of the equilibrium free energies by TFE is already explicit in the model of eq 1.) Extrapolating these kinetics to the limit of 0% TFE then gives the folding and unfolding rates in water at 25 °C (Figure 7):

$$k_u(aq) = 3.3 \pm 0.5 (\mu s)^{-1}$$

$$k_f(aq) = 0.30 \pm 0.04 (\mu s)^{-1}$$

$$k_{relax} = k_u + k_f = 3.6 \pm 0.5 (\mu s)^{-1}$$

Evidently IA₃ folds rather slowly in comparison to many helix-forming model peptides, such as alanine peptides, which often display submicrosecond kinetics (e.g., $1/k_f \approx$ 200 ns).[35,37−39] Some model peptides even show indications of rates as fast as 2×10^7 s^{-1}.[40] By comparison to such molecules, IA₃ (in the

(35) Huang, C. Y.; Getahun, Z.; Wang, T.; DeGrado, W. F.; Gai, F. *J. Am. Chem. Soc.* **2001**, *123* (48), 12111–12112.

(36) Huang, C. Y.; Getahun, Z.; Zhu, Y.; Klemke, J. W.; DeGrado, W. F.; Gai, F. *Proc. Natl. Acad. Sci. U.S.A.* **2002**, *99* (5), 2788–2793.

(37) Thompson, P. A.; Eaton, W. A.; Hofrichter, J. *Biochemistry* **1997**, *36* (30), 9200–9210.

(38) Williams, S.; Causgrove, T. P.; Gilmanshin, R.; Fang, K. S.; Callender, R. H.; Woodruff, W. H.; Dyer, R. B. *Biochemistry* **1996**, *35* (3), 691–697.

(39) Dyer, R. B.; Gai, F.; Woodruff, W. H. *Acc. Chem. Res.* **1998**, *31* (11), 709–716.

(40) Causgrove, T. P.; Dyer, R. B. *Chem. Phys.* **2006**, *323* (1), 2–10.
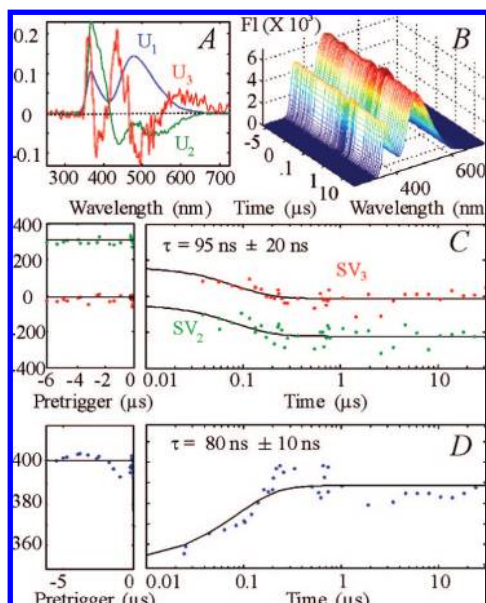
Figure 8. Fluorescence relaxation of a sample containing YPrA (50 μM) equilibrated with single-labeled K16C-dansyl IA₃ (40 μM) in pH 4.5 acetate buffer, triggered by a laser temperature jump (from $T = 17.3$ to 23.8 °C at $t = 0$). The signal consists of emission at 500 nm from the dansyl acceptor on the IA₃ peptide and 350 nm emission from the native tryptophan residues of YPrA. (A) Three significant components $U_1(\lambda) - U_3(\lambda)$ are obtained in the spectral decomposition of the emission spectra (B). (C) The time courses $SV_2(t)$ and $SV_3(t)$ (associated with $U_2(\lambda)$ and $U_3(\lambda)$ respectively) show a relaxation on the time scale $\tau = 95 \pm 20$ ns. (D) An independent (photomultiplier) measurement of the Trp emission during the experiment shows a rise in Trp fluorescence on the time scale $\tau = 80 \pm 10$ ns.

absence of YPrA) is a poor folder, with sluggish or inefficient nucleation of the helix and a poorly stabilized helical state.

Relaxation Kinetics of IA₃/YPrA. We also examined the relaxation of the complex formed by IA₃ peptide (the single-labeled K16C-dansyl mutant) and YPrA, in response to a laser *T*-jump. These relaxation kinetics are difficult to measure, as the very tight binding interaction between the protease and the peptide leads to a relaxation signal of small amplitude. In order to minimize interference from dansyl fluorescence of free IA₃, and direct excitation of the dansyl moiety, a slight excess of protease was used in these studies. (The excess protease does not degrade the sample on the 1−3 h time scale of the *T*-jump measurements.) At experimental conditions of 50 μM protease concentration, a 40 μM peptide concentration, and an inhibition constant $K_I \approx 1$ nM, the binding equilibrium lies far toward the bound/inhibited state, with only ∼4 nM free peptide and ∼10 μM free protease. The temperature perturbation triggers reequilibration between the complex and the dissociated state. However, the number of molecules involved can be small and hence the relaxation signal quite weak. Nevertheless the *T*-jump triggers a concurrent relaxation at both the tryptophan and dansyl emission wavelengths. Figure 8 shows the time-resolved fluorescence spectra obtained following a temperature-jump from an initial temperature of 17.3 °C to a final temperature of 23.8 °C. The CCD detector (recording spectral shifts at both the Trp and dansyl wavelengths) recorded a relaxation on a time scale $\tau = 95 \pm 20$ ns, while the photomultiplier (detecting Trp emission only) recorded a relaxation time $\tau = 80 \pm 10$ ns, to give a weighted average of $\tau = 83 \pm 9$ ns for the relaxation time.

There are several indications that this fast process must represent an interaction between the peptide and protease (see

Discussion). Signal-to-noise constraints prevented us from measuring the dependence of the rate of the fast relaxation on the concentration of IA₃. Instead we were limited to roughly 50 μM YPrA and comparable values for the IA₃ concentration. At lower IA₃ concentrations the fluorescence relaxation signal is weak. At higher IA₃ concentrations direct excitation of the dansyl acceptor by the UV laser generates a fluorescence signal background that obscures the relaxation signal.

Discussion

Although coupled folding and binding is known to play a role in many protein/ligand interactions, few studies have provided insight into the actual sequence of events that occurs during the interaction. Theoretical studies have suggested some potential mechanisms for coupled folding and binding and have explored particular examples. Verkhivker et al. used simulation to characterize the transition state ensemble for the interaction of the intrinsically disordered *p27* protein with the Cdk2 complex,[41] and Lu et al. simulated the energy surface for the folding of the CBD protein fragment to CdC42.[42] However there have been few attempts to characterize experimentally the mechanism of coupled folding and binding in particular systems.[14−17] Cofactor-assisted protein folding is one case that has been studied:[16,43] Muralidhara et al.[16] found that unfolded flavodoxin binds its flavin mononucleotide cofactor rapidly, and that the presence of the bound cofactor accelerates the folding of the protein by roughly 12-fold. We are aware of relatively few experimental studies of the effect of protein−protein binding on the rate of folding. Sugase et al. found evidence that the intrinsically unstructured pKID domain of the transcription factor CREB forms an encounter complex with its target, the KIX domain of the CREB binding protein, and that this encounter complex contains numerous nonspecific or nonfolded interactions. This suggests that weak nonspecific binding precedes actual folding.[14] Onitsuka et al.[15] have very recently reported on intrinsically disordered mutants of staphylococcal nuclease (SNase), whose folding is induced by ligand binding. These authors found that a particular SNase mutant appeared to fold before binding the ligand, while another mutant appeared to fold after binding the ligand. The folding of a dimeric coiled-coil helix protein derived from GCN4 has been studied by Meisner and Sosnick,[17] who found that folding occurred faster than would be expected for the collision of two preformed helices (a scenario akin to Scheme 1 above), suggesting that interaction of the unstructured chains preceded folding. Therefore one of the simplest questions one can ask about the mechanism of the IA₃−YPrA interaction is whether folding of IA₃ precedes or follows its initial contact with the YPrA target. "Conformational selection" is one simple model (Scheme 1) in which a small fraction of free IA₃ molecules transiently fold to the helical state in aqueous solution, producing a folded subpopulation that is able to bind rapidly to the YPrA active site. An alternative is a "flycasting" model[12] in which the disordered IA₃ molecule makes contact with the protease, and interactions with protease then provide steering forces to guide the peptide toward its helical fold (Scheme 2). Our study of the folding kinetics of the intrinsically disordered IA₃, both in

(41) Verkhivker, G. M.; Bouzida, D.; Gehlhaar, D. K.; Rejto, P. A.; Freer, S. T.; Rose, P. W. *Proc. Natl. Acad. Sci. U.S.A.* **2003**, *100* (9), 5148–5153.
(42) Lu, Q.; Lu, H. P.; Wang, J. *Phys. Rev. Lett.* **2007**, *98*, 128105.
(43) Crespin, M. O.; Boys, B. L.; Konermann, L. *Febs Lett.* **2005**, *579* (1), 271–274.

the presence and the absence of the YPrA target, allows us to draw some conclusions about the merits of these two models.

We measured both the rate of folding of the free IA$_3$ peptide and the relaxation kinetics of the peptide-protease interaction complex. 2D ^{15}N-HSQC spectroscopy and far-UV circular dichroism (CD) studies have established that free IA$_3$ has little helical character in aqueous solvent,[22,23] although its N-terminal 34 residues form an α-helix in the inhibition complex with YPrA. Addition of a 2,2,2-trifluoroethanol (TFE) cosolvent stabilizes the helical state of free IA$_3$ so that its folding rate can be measured. Residue-specific analysis of 2D ^{15}N-HSQC spectra shows that TFE promotes helix formation *via* a two-state transition, and that the helix forms in virtually the same N-terminal residues that comprise the helix in the YPrA-IA$_3$ inhibition complex.[22] Equilibrium CD spectra of IA$_3$ (and several labeled mutants) over a range of solvent and temperature conditions allowed us to construct a simple free energy model for the helix-coil transition, so that laser *T*-jump fluorescence spectroscopy could then be used to measure the folding and unfolding rates of free IA$_3$ as a function of TFE concentration. Extrapolation of these rates to aqueous conditions then provided the helix formation rate of free IA$_3$ in water. When the IA$_3$/YPrA complex is subjected to a temperature jump perturbation (in water), the fluorescence of both the FRET donor (Trp in YPrA) and the acceptor (dansyl-IA$_3$) respond in a single relaxation with $\tau = 80-90$ ns, indicating a shift in equilibrium that is significantly faster than either the folding (~3.3 μs) or unfolding (~300 ns) of IA$_3$ alone in water.

From its rate and wavelength properties it does not appear that this rapid relaxation signal could arise from either the IA$_3$ alone or the protease alone. First, it contains a signal component at the dansyl wavelength, while the dansyl was attached to the IA$_3$ only. Likewise it contains a signal component at the tryptophan wavelength, and the Trp residues were located on the protease. The observed relaxation is probably also too rapid to result from folding or unfolding of free IA$_3$ in the sample; it is more than three times faster than our (extrapolated) folding/unfolding rate for free IA$_3$ in aqueous solvent. Furthermore, the thermodynamic data indicate that a moderate temperature jump will not significantly perturb the folding/unfolding equilibrium of free IA$_3$ in the absence of TFE. In fact, in a control experiment where the free single-labeled K16C-dansyl IA$_3$ was subjected to a *T*-jump (in the absence of protease and TFE), no relaxation signal is observed at either the dansyl or tryptophan wavelengths. This implies that the relaxation is not attributable to either the peptide alone or the protease alone. Instead it appears that both the protease and its inhibitor participate in the 80–90 ns process. The relaxation must signal a rapid change in the spatial separation or relative orientation of the YPrA Trp residues and the IA$_3$ dansyl label.

Furthermore, given the rapid time scale of this relaxation it appears very unlikely to represent a simple two-state association or dissociation interaction between free IA$_3$ and the protease. For $K_I \approx 1$ nM, peptide and protease concentrations of 40 μM and 50 μM respectively, and a relaxation time of $\tau = 80-90$ ns, the association (k_{on}) and dissociation (k_{off}) rates in the simplest on/off binding model should obey $k_{off}/k_{on} = K_I$ and $k_{off} + [YPrA]_e k_{on} = 1/\tau$. Here $[YPrA]_e \approx 10$ μM is the excess protease concentration. This leads to a large estimate, $k_{on} = (1/\tau)(K_I + [YPrA]_e)^{-1} \approx 10^{12}$ $(M\ s)^{-1}$, for the rate of bimolecular association. This result is unphysical, as it exceeds

a diffusion-limited association rate, $k_D \approx 10^9$/M s,[44] by several orders of magnitude. A similar logic argues against a three-state model like Scheme 1, in which the bimolecular process is the association of the folded IA$_3$ helix with the protease. An unphysically high rate of association k_{on} is required in order to generate a submicrosecond, bimolecular process at low peptide concentrations. Our data therefore appear to rule out Scheme 1 for the mechanism of coupled folding and binding. Alternatively, the observed relaxation could indicate a fast reorientation of IA$_3$ chains that are already in contact with the protease. However, this is essentially a different model for the interaction (i.e., Scheme 2).

In Scheme 2 the bimolecular association of free peptide (I) and proteinase (Y) produces an encounter complex (E) prior to formation of the inhibited complex (C). The observed rise in Trp emission signals either a dissociation of the encounter complex (the bimolecular step $E \rightarrow Y + I$) or a loss of contact between the folded IA$_3$ helix and the proteinase active site ($C \rightarrow E$). Here as in Scheme 1 the 80–90 ns relaxation appears to be too rapid to represent the bimolecular process. If it is a signature of the initial bimolecular association between unfolded IA$_3$ and YPrA, then the rate of association (k_{on}) and dissociation (k_{off}) would have to satisfy (roughly) $k_{on}[YPrA]_e + k_{off} \approx 10^7$ s^{-1}, where the excess proteinase concentration is $[YPrA]_e \approx 10$ μM. This requires either $k_{on} \approx 10^{12}$ $(M\ s)^{-1}$ or $k_{off} \approx 10^7$/s. The k_{on} value should be ruled out as it exceeds the diffusion-limited rate for a pair of proteins. The k_{off} value seems possible in principle, although it is exceptionally fast (in comparison with other protein–ligand systems) and would lead to a remarkably weak association of the unfolded IA$_3$ and the YPrA, unless k_{on} is also quite fast: e.g. $K_D \approx 1$ M if $k_{off} \approx 10^7$ /s and $k_{on} \approx 10^7$ $(M\ s)^{-1}$. Such a combination of extraordinarily rapid kinetics and weak association would make it difficult to explain the potent inhibition ($K_I < 1$ nM) of YPrA by IA$_3$. For example, even for diffusion-limited association $k_{on} \approx 10^9$ $(M\ s)^{-1}$, a dissociation rate $k_{off} \approx 10^7$ /s gives $[I][Y]/[E] \approx k_{off}/k_{on} \approx 10^{-2}$ M. Achieving nanomolar inhibition would then require that the $E \leftrightarrow C$ equilibrium favor C over E by a factor $\sim10^7$. Since free IA$_3$ in water is only $\sim10\%$ helix, this would require that assocation with the proteinase enhance the folded/unfolded population ratio for the IA$_3$ helix by 8 orders of magnitude. A slightly more credible—but still very fast—association rate $k_{on} \approx 10^7$ $(M\ s)^{-1}$ would require that C is favored over E by a factor $\sim10^9$, for a net enhancement of 10^{10} in the folded/unfolded ratio for IA$_3$. These estimates seem implausible, as they imply subpicomolar occupation of the intermediate state C under our conditions, they raise the question of how any signal could be detected, and they certainly contradict what is known about other protein interaction rates and other coupled binding/folding systems. For example, Sugase et al., in their three-site analysis of the association of the *p27* IDP with its CREB binding protein target, found rather uniform rates for the initial association (average $k_{on} \approx 6 \times 10^6$/M s) but more variable—and generally quite slow—kinetics for the dissociation step: 10 s^{-1} $< k_{off} < 100$ s^{-1} for most residues.

Such arguments strongly disfavor interpreting the 80–90 ns relaxation as the bimolecular step in Scheme 2. The signal therefore appears much more likely to be the folding/unfolding step in Scheme 2: specifically, the rise in the Trp emission signal indicates that the process involves an increase in the donor–acceptor separation, such as unfolding and detachment of the IA$_3$ helix

(44) Northrup, S. H.; Erickson, H. P. *Proc. Natl. Acad. Sci. U.S.A.* **1992**, *89* (8), 3338–3342.

at the YPrA active site. The rate of the observed relaxation is nearly three times faster than our estimate for the folding/unfolding relaxation of free IA$_3$ ($\tau \approx 260 \pm 30$ ns in water), which implies that the proximity of the enzyme substantially accelerates the kinetics of IA$_3$ folding/unfolding. If the helical state C in Scheme 2 is strongly favored over the intermediate state E (in order to give subnanomolar inhibition of the YPrA active site), then the 80−90 ns relaxation must be dominated by the rate of IA$_3$ folding, *i.e.* $k_f \gg k_u$ with $k_f + k_u \approx (80-90$ ns$)^{-1}$ so that the folding rate of IA$_3$ in contact with YPrA is roughly $k_f \approx (80-90$ ns$)^{-1}$. Hence interaction with the proteinase appears to accelerate the folding of IA$_3$ by $\sim 30 \times$ relative to the rate in free solution, to give a folding rate that is comparable to the fastest helix-folding observed in model peptides.[35,37−40] For fairly typical rates for the initial bimolecular association and dissociation in Scheme 2 (e.g., $k_{on} \sim 10^6$ (M s)$^{-1}$ and $k_{off} \approx (1-100)$ s^{-1}, for which $k_{off}/k_{on} \approx 10^{-4}-10^{-6}$ M), the estimate $k_f \sim (80-90$ ns$)^{-1}$ and $K_I < 1$ nM together imply $k_f/k_u \approx 10^3-10^5$; this should be compared to the stability of this helix in water, $k_f/k_u \approx 0.1$ (Figure 4). That is, the inhibitory contacts with YPrA provide a template for the folding of the IA$_3$ helix that accelerates 30-fold the nucleation of the helix and improves its stability by about 22−34 kJ/mol.

Conclusions

We have combined kinetic and equilibrium studies to investigate the mechanism of the coupled folding and binding interaction in which the intrinsically disordered peptide IA$_3$ inhibits its target proteinase YPrA. Our results favor a model (Scheme 2) in which the unfolded IA$_3$ first forms a weak complex with YPrA, prior to forming the helix that inhibits the enzyme. Our study does not provide direct information about the intermolecular interactions that stabilize that intermediate state. Although it is well-established that the inhibitory potency of the 68-residue IA$_3$ resides in its N-terminal (i.e., helix-forming) 34 residues, and that nanomolar inhibition is retained when the C-terminal residues are absent,[25] it is still conceivable that residues outside the helix-forming region of IA$_3$ interact with residues on the surface of the proteinase, away from the active site. There is some precedent for this in the observation that extension of the IA$_3$ peptide at the N-terminus broadens

its range of inhibition to include other aspartic proteinases.[45] However, deletion or mutation of the C-terminus did not have such effects in that study. More significantly, an NMR study found that the ^{15}N HSQC peaks of three glycine residues of the C-terminus of IA$_3$ (G40, G62, and G64) broadened and then vanished as substoichiometric amounts of YPrA were titrated into IA$_3$.[23] These residues lie well outside the helix-forming YPrA binding domain. This finding suggests an intermediate exchange, in which the disordered C-terminus of IA$_3$ intermittently interacts with YPrA. It is intriguing to consider that the C-terminal residues of IA$_3$ can have measurable interactions with YPrA and yet have no significant impact on the equilibrium constant for inhibition. One may speculate that the intermediate complex in Scheme 2 is an association between YPrA and the C-terminus of IA$_3$, where the N-terminal residues do not participate. This is essentially a fly casting model[12]—an intermediate state of interaction between the disordered peptide and its target that facilitates the dynamics of folding and binding without changing the equilibrium constant.

These findings suggest several directions for future work. For example, it may be quite interesting to explore the role of crowding *in vivo* on coupled folding-binding interactions of this type. It will certainly be important to obtain a residue-level description of the binding mechanism and the intermediate state. Coarse-grained computer simulations can probe dynamics of conformational changes at the level of a whole protein or complex,[46] and such simulations on this sytem could potentially provide useful detail. Future experimental studies will need to explore the IA$_3$ C-terminal residues, lying outside the helix-forming region, through mutational studies designed to pinpoint the particular interactions that stabilize the binding intermediate.

Supporting Information Available: Complete ref 11. This material is available free of charge via the Internet at http://pubs.acs.org.

JA803221C

(45) Winterburn, T. J.; Phylip, L. H.; Bur, D.; Wyatt, D. M.; Berry, C.; Kay, J. *FEBS J.* **2007**, *274*, 3685–3694.
(46) Lu, Q.; Wang, J. *J. Am. Chem. Soc.* **2008**, *130* (14), 4772–4783.